Laser Ablation of Thin Metal Layers and Foils

G. Rodriguez[a], A. R. Valenzuela[a] and S. A. Clarke[b]

a) Materials Physics and Applications Division, MPA-CINT
b) Weapons Systems Division, W-6

Los Alamos National Laboratory,

Los Alamos, NM 87545

Heterodyne Workshop – Livermore, July 20-21, 2006

Outline

- Background & Motivation
- PDV Heterodyne System Description
- Results
- Analysis Techniques

Introduction

We seek to understand when a laser ablates a thin metal layer, how the subsequent plasma and ejected material evolves in time. To do this our tasks are to:

- Perform hydrodynamic simulations
- Experimentally measure the velocity of the ablated metal with temporal resolution (PDV).
- Experimentally detect the shape of the ablated metal with temporal resolution (Schlieren and DOTS topographic imaging).
- Create a feedback loop to use experimental data to refine the hydrodynamic simulations

We show that PDV inherently detects velocity field distribution of ejected material/particles that are otherwise nearly impossible using VISAR techniques.

Laser Ablation Geometry

- We study the interaction between a short laser pulse (λ = 1064 nm, 8 ns – 60 ns) with a variety of thin metal (Ti, Al, Au) targets:

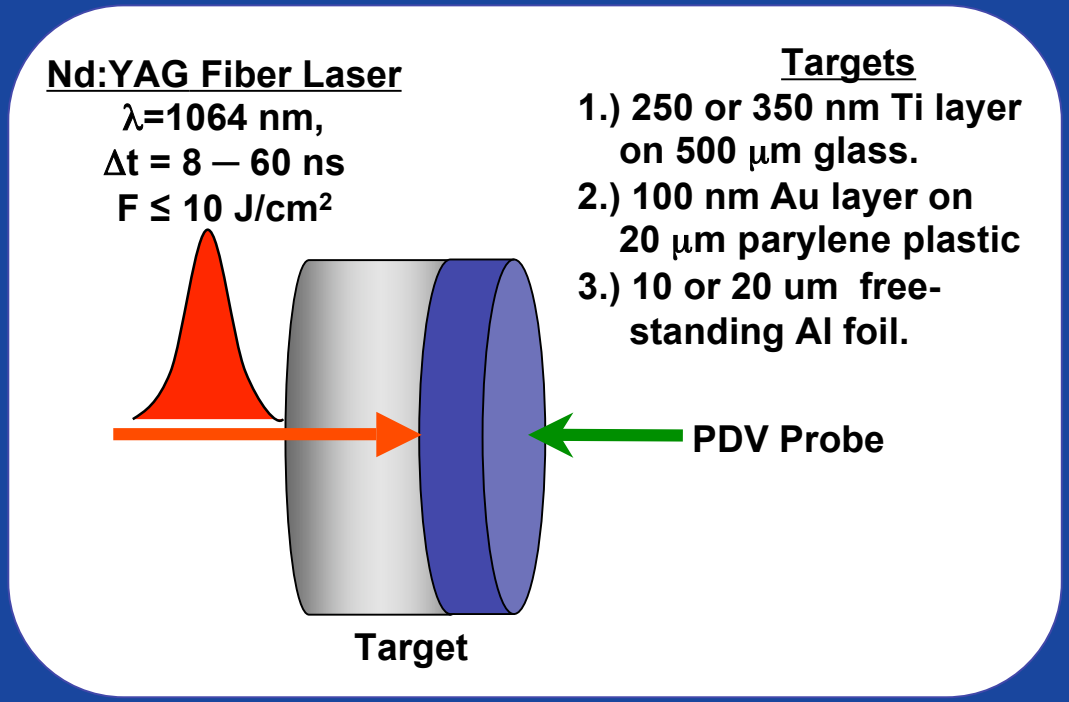

Ablation Example: 250 nm Ti layer on 500 μm thick fused silica substrate.

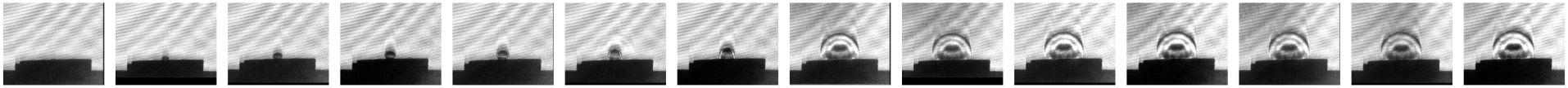

Ti ablation Schlieren movie

- 14 Frames
- Frame Exposure Time: 5 ns
- Interframe Time: 50 ns

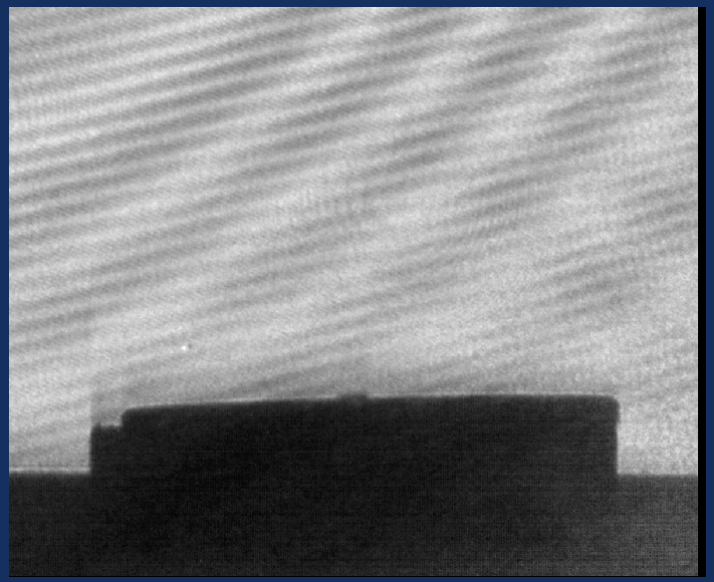

Picture of laser-ablated fused silica/Ti plate

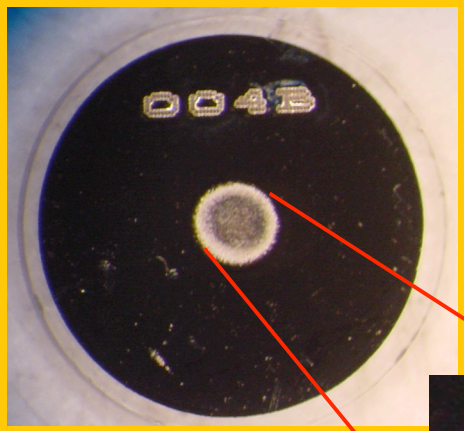

5 mm diameter plate

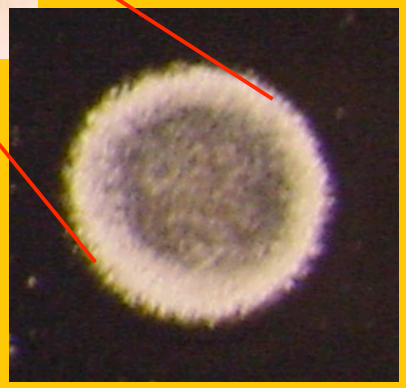

625 μm ablation spot

4-Channel PDV System

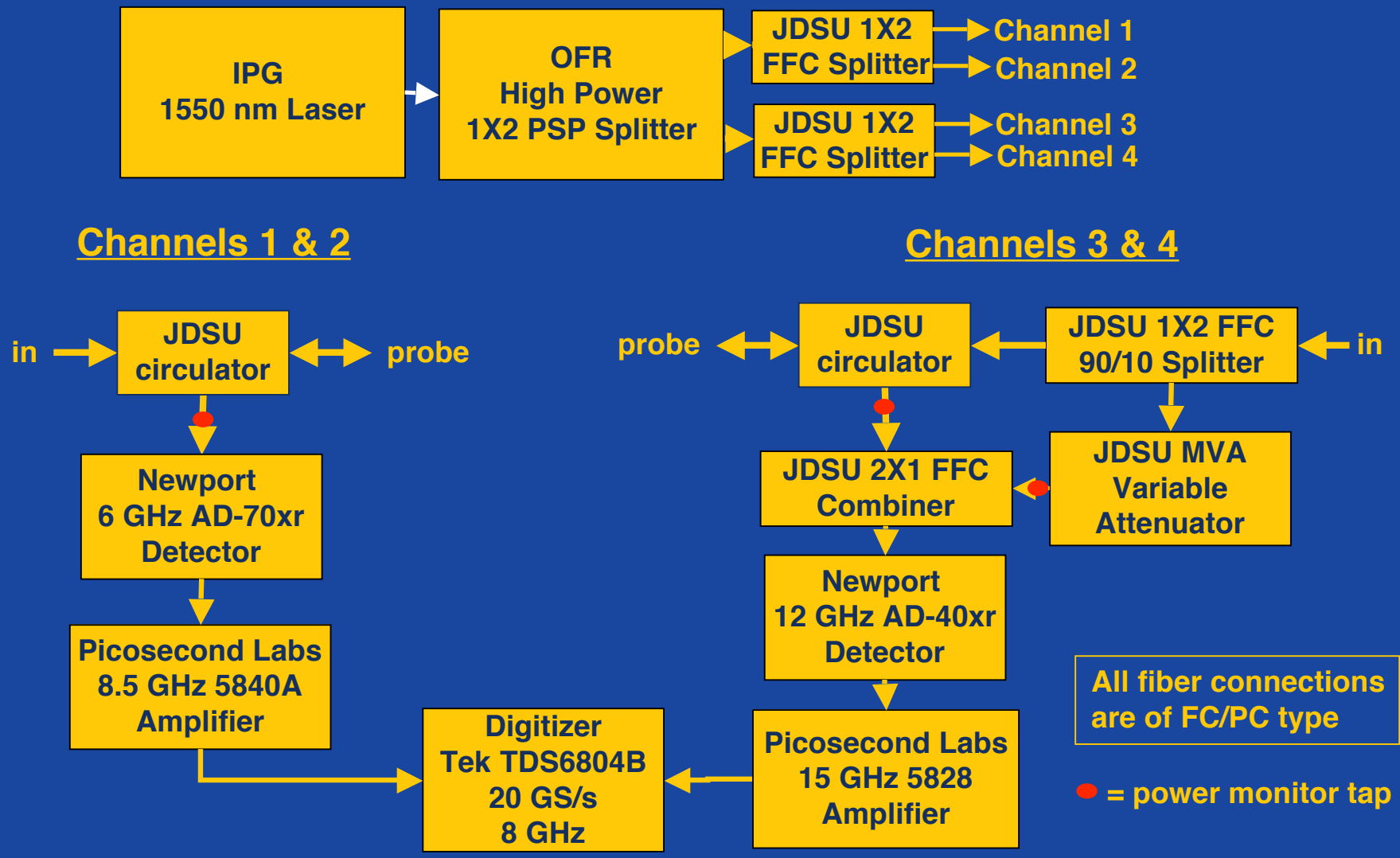

4-Channel PDV System

PDV Rack

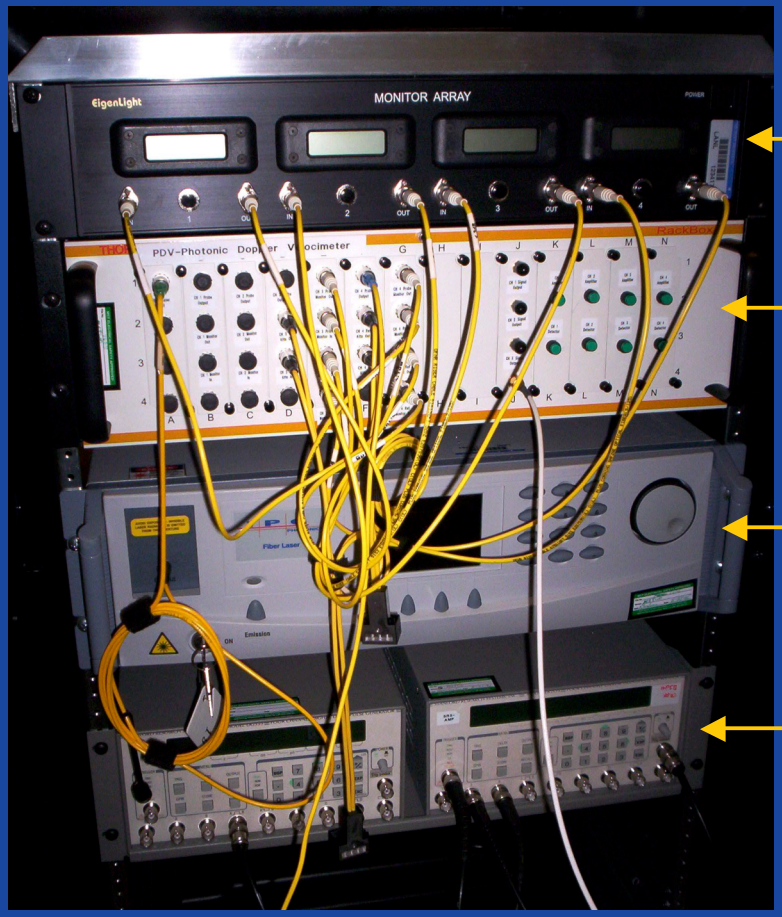

Eigenlight Power Monitor Array

Fiber Optics, Detector and Amplifier Chassis

2W IPG Laser

Trigger & Timing Delay Generators

Experimental Setup & Probes Used

Setup

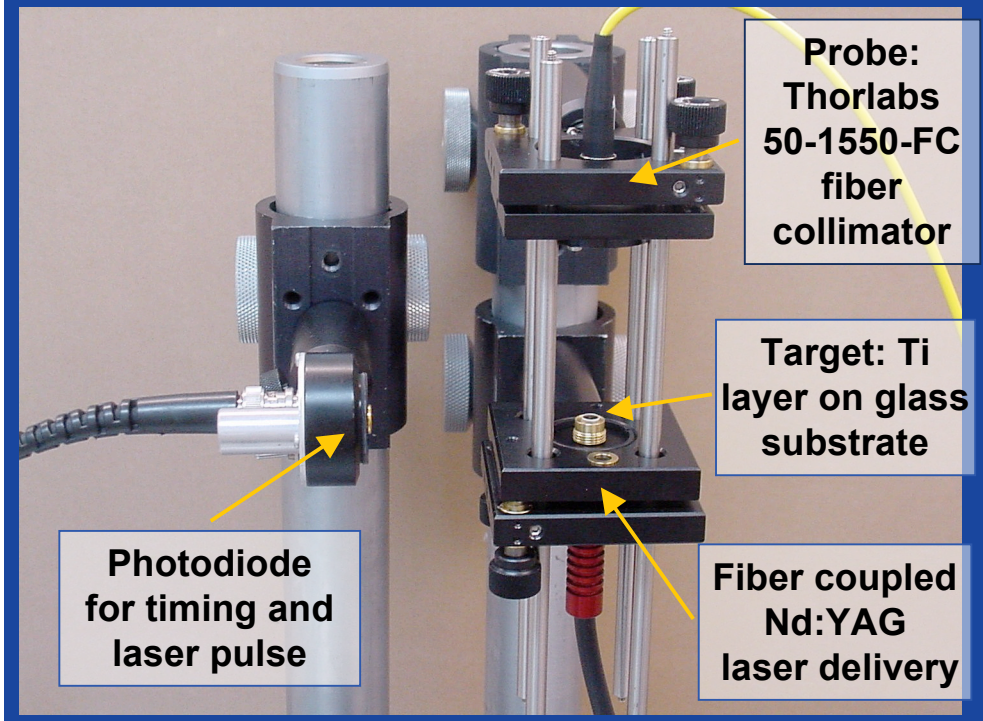

Probes

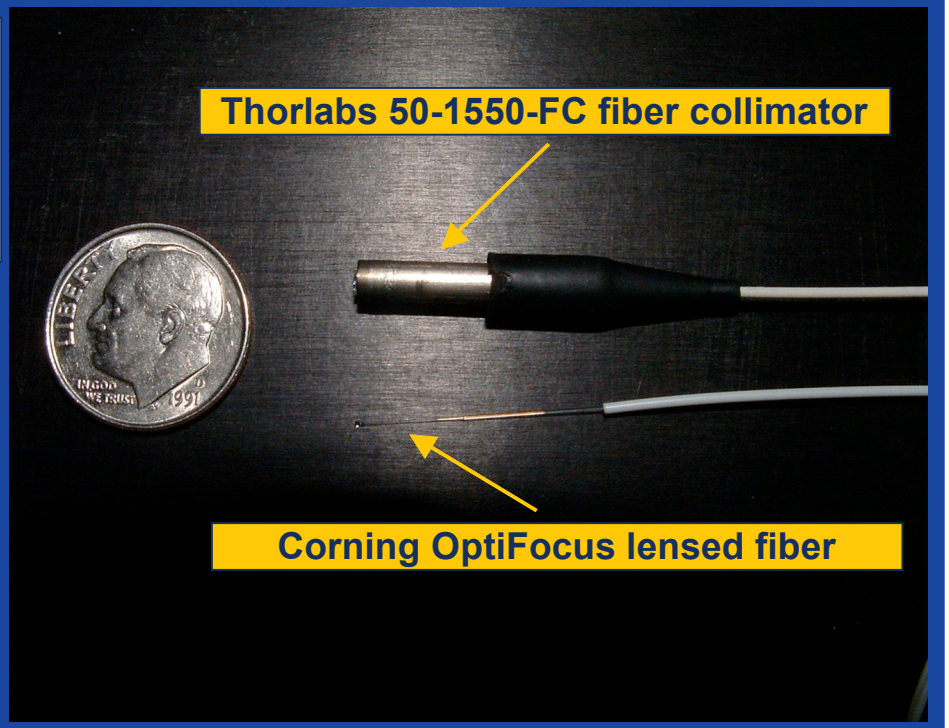

Thorlabs collimated fiber: 500 μm spot @ inches away
Corning lensed fiber: 60 μm spot @ 2.5 mm focal length

Results: Sample Temporal Waveforms and STFT Spectrograms

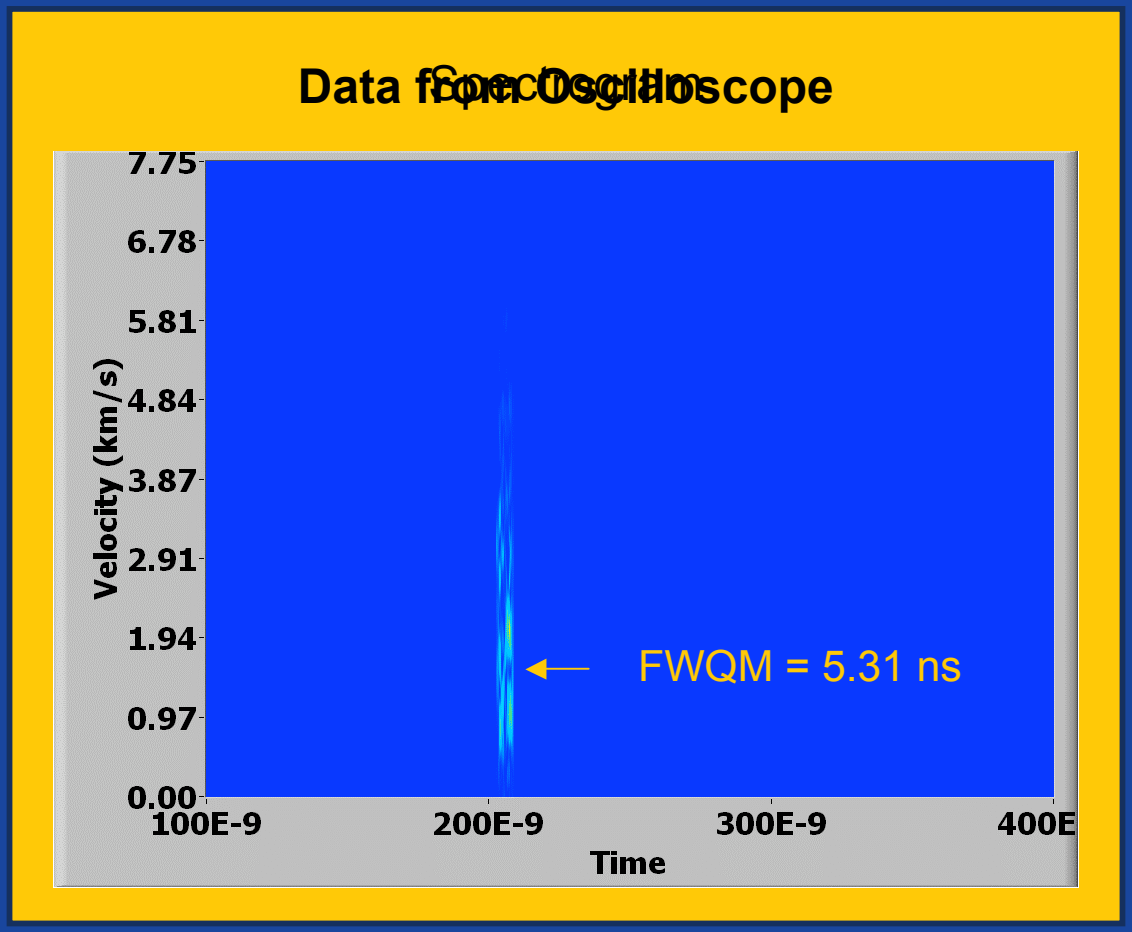

Deconstructing Spectrograms

Spectrogr profiles.

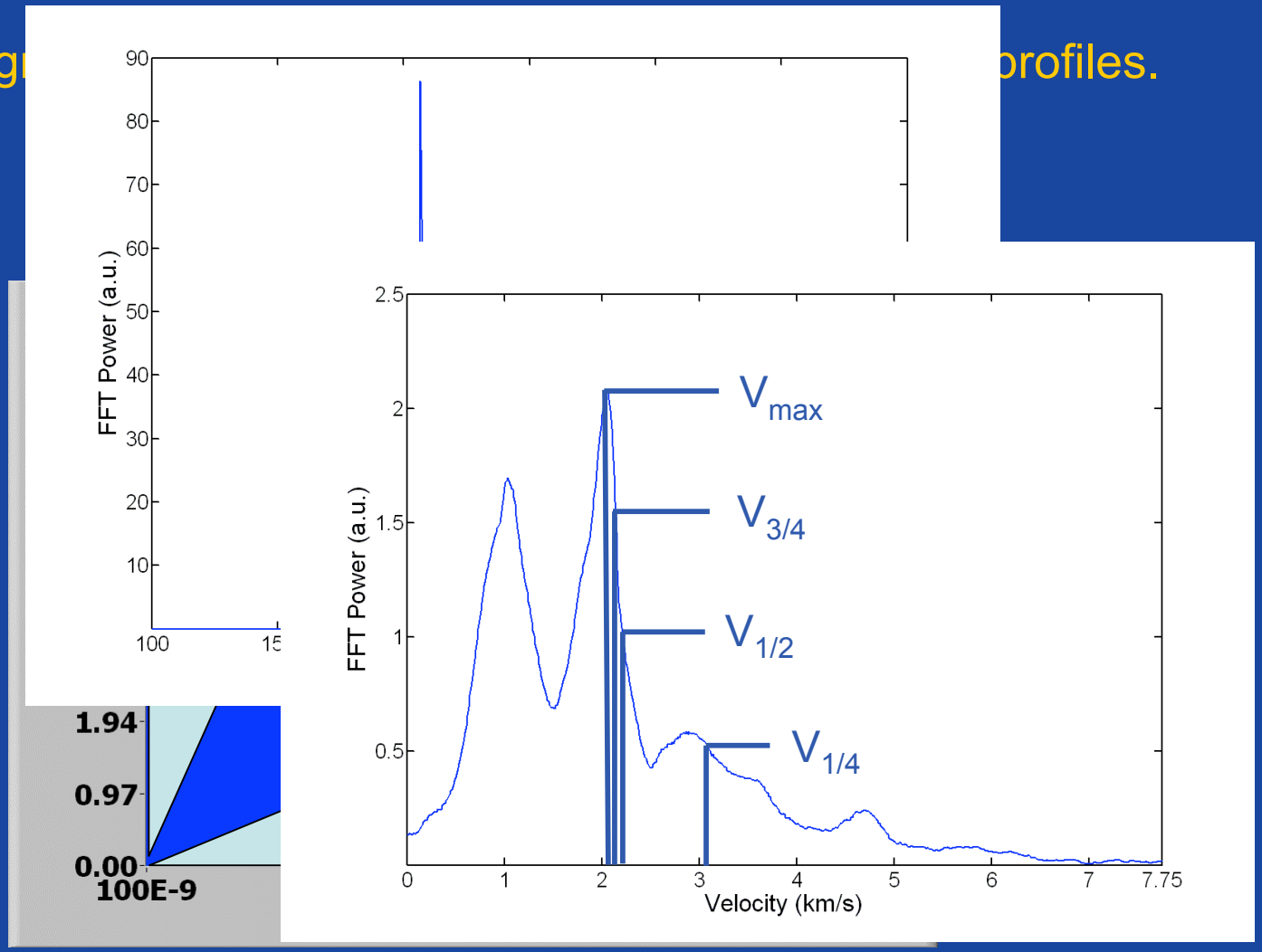

Laser ablation rate is tracked by PDV

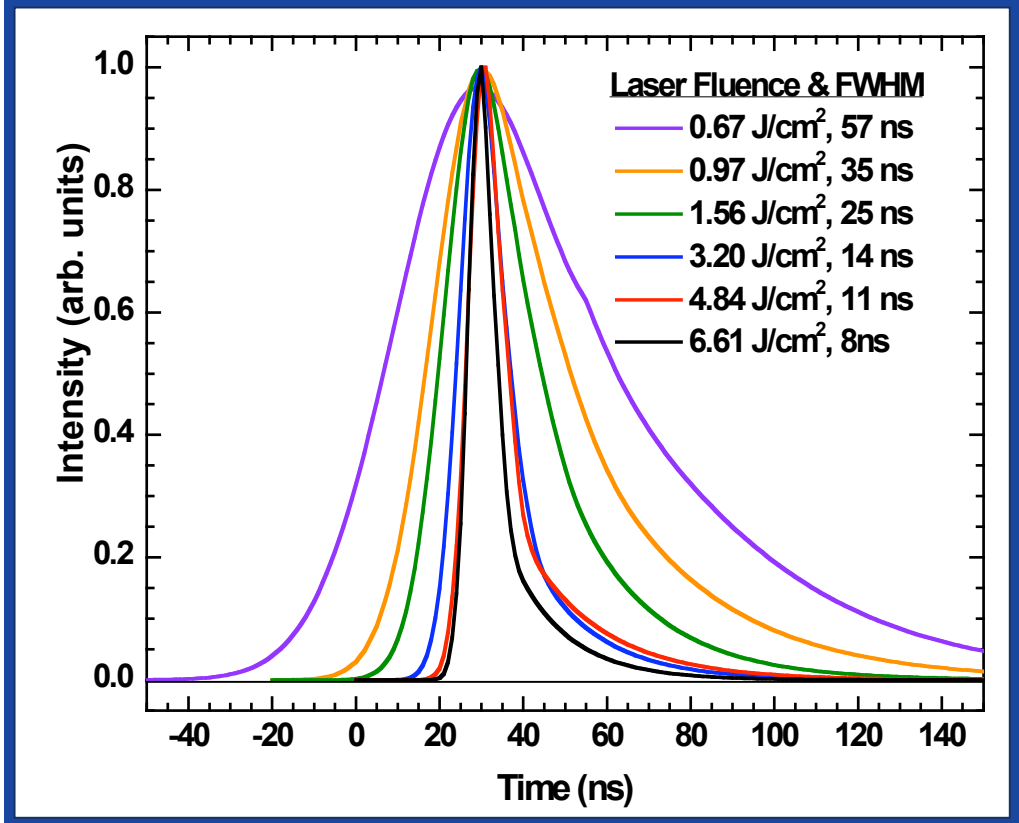

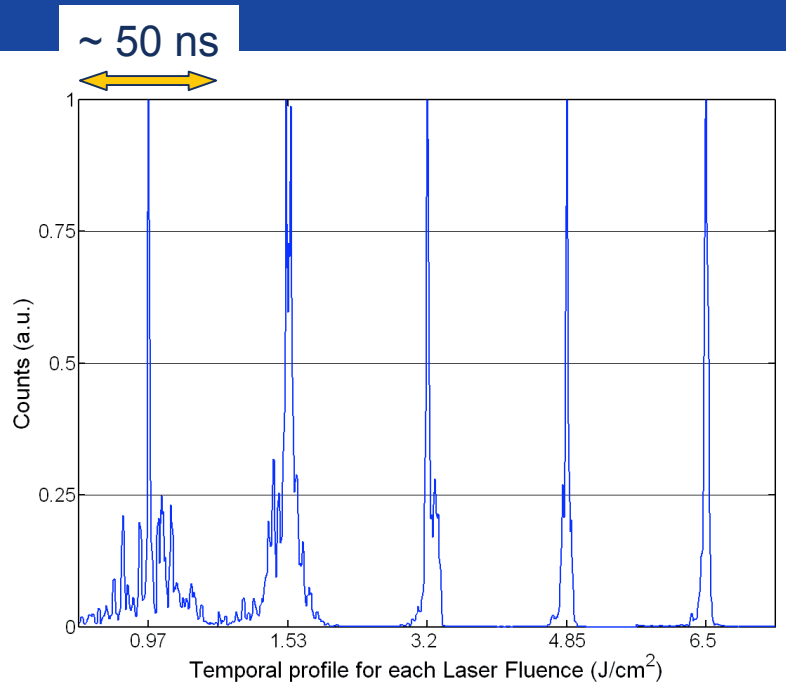

Laser Pulse Duration vs. PDV FWHM & FWQM

PDV temporal signatures fall in line with driving laser pulse duration.

350 nm

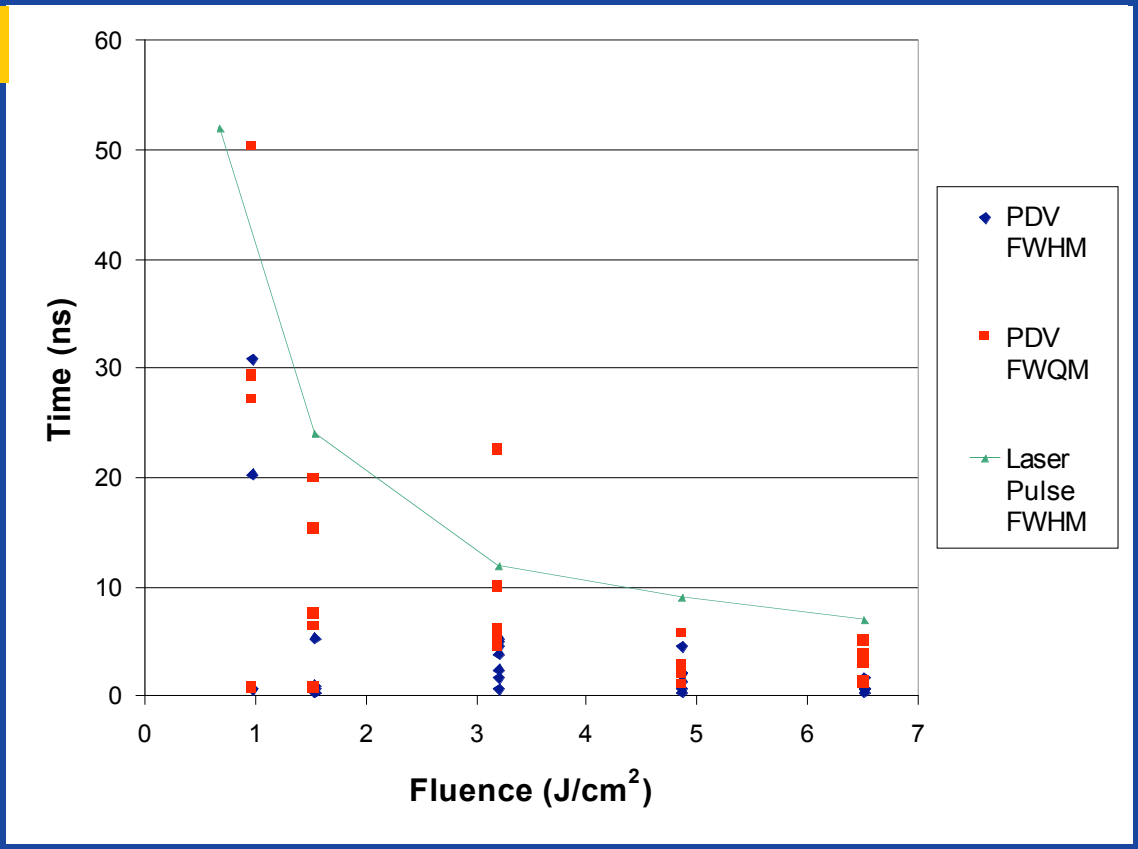

Velocity Profiles vs. Laser Fluence

Broadening velocity distribution with increasing laser fluence

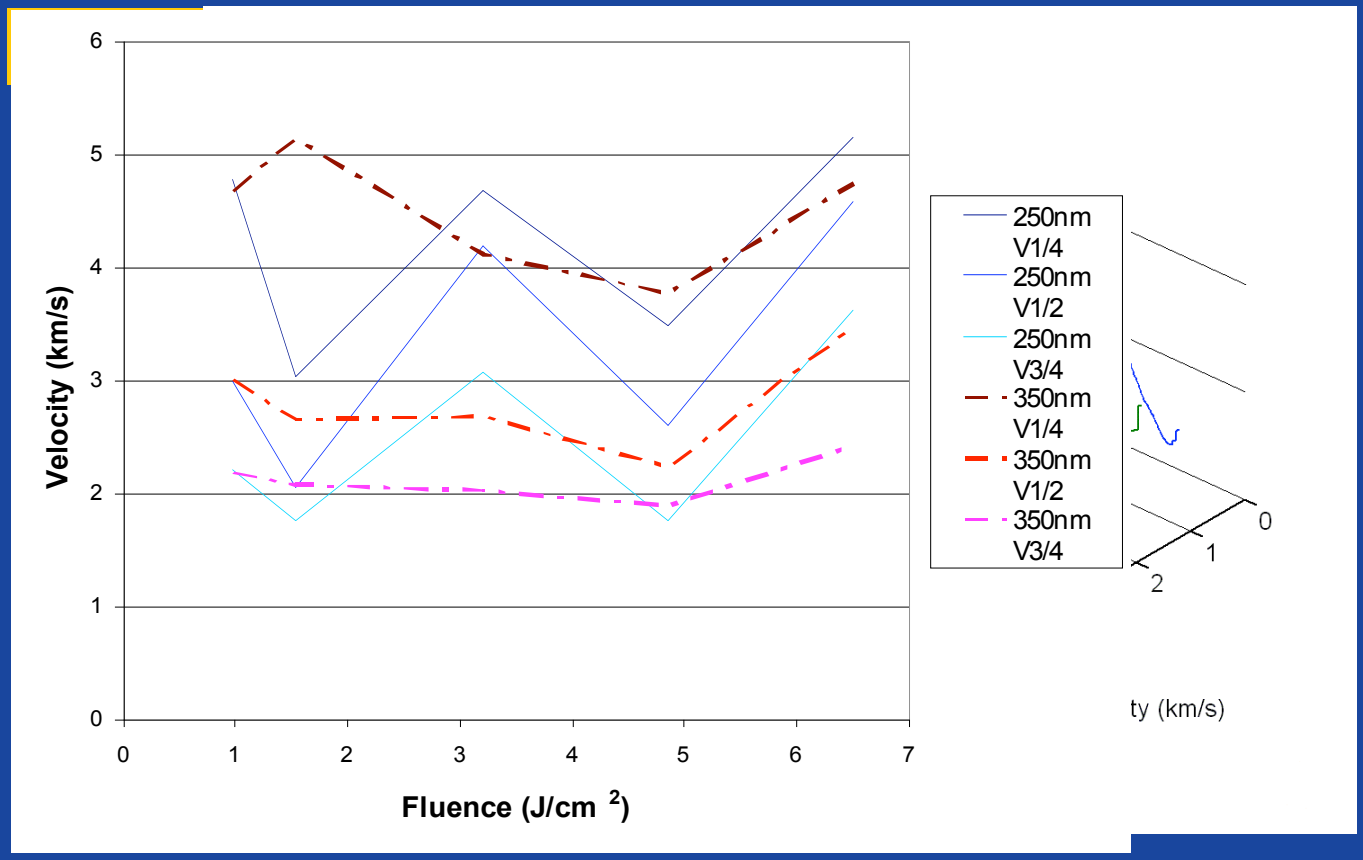

OptiFocus Fiber Lens

- OptiFocus Lens provides smaller focal spot on Ti surface

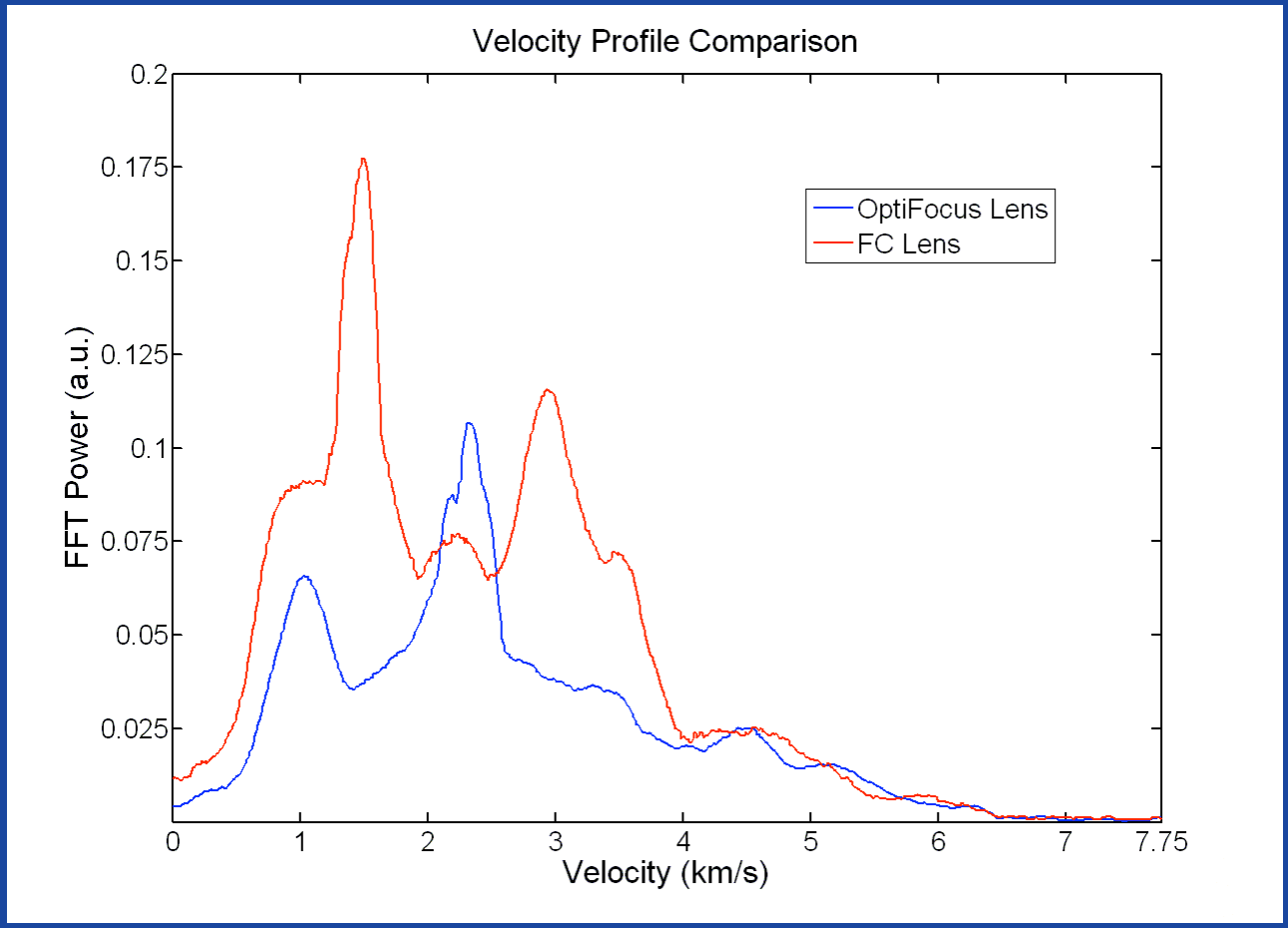

Higher Bandwidth Differences

- Bandwidth increase of $$$ between LBW and HBW

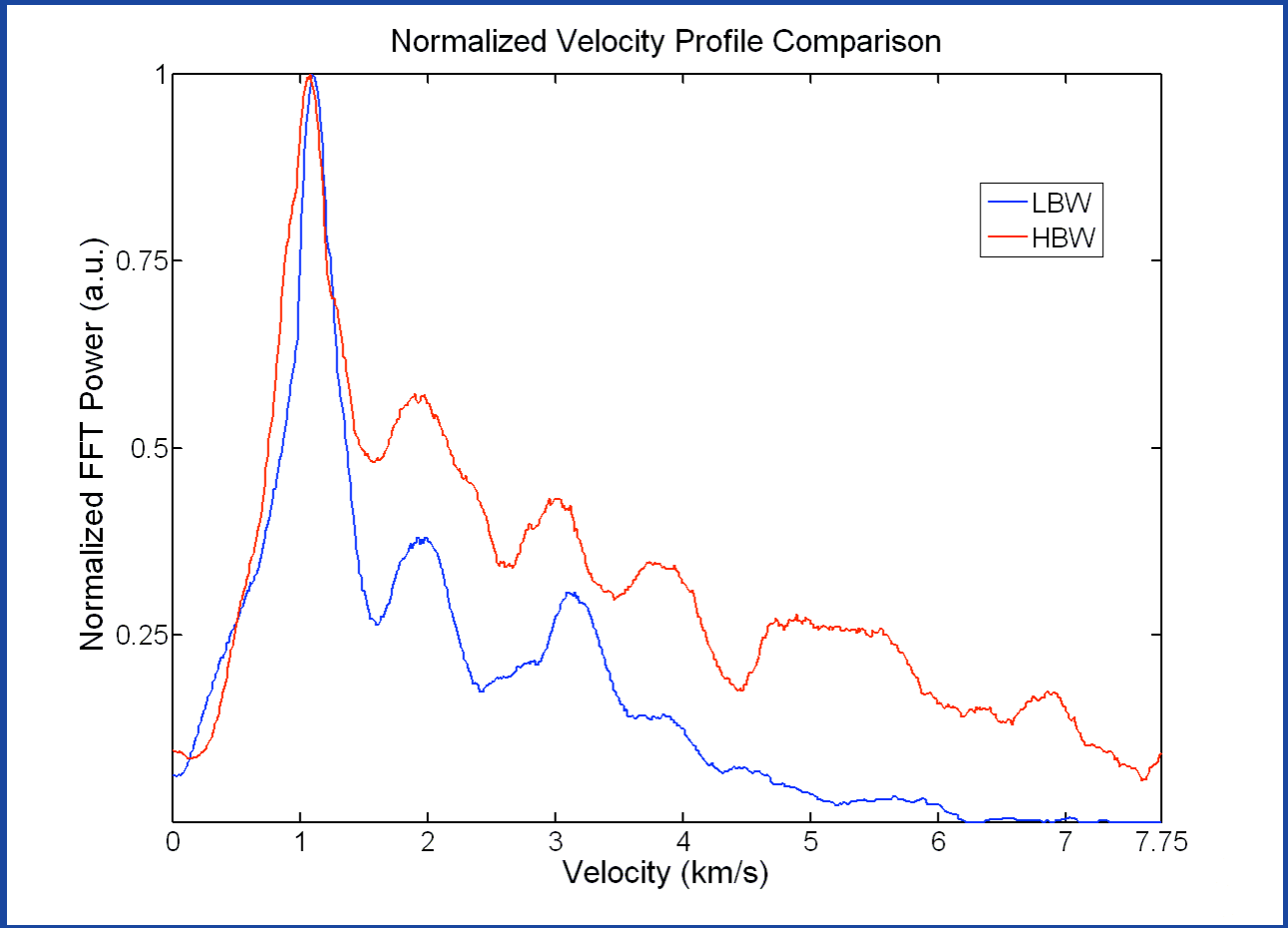

Expansion Velocity vs. Laser Fluence

- PDV measurements detect a distribution of particle velocities from with the field of view of the collection optic.
- Velocity spectrograms show an increase in velocity distribution and a narrowing in time observation window as the fluence increases → Consistent with a quickening of the ejected material as the energy deposition rate increases.
- Peak velocity in the distributions are consistent with HYADES calculations (i.e., at $F \sim 4$ J/cm^2, $v_{peak} > 5$ μm/ns).

PDV on Au Target

Performed PDV measurements on 100 nm of Au on 20 μm of Parylene.

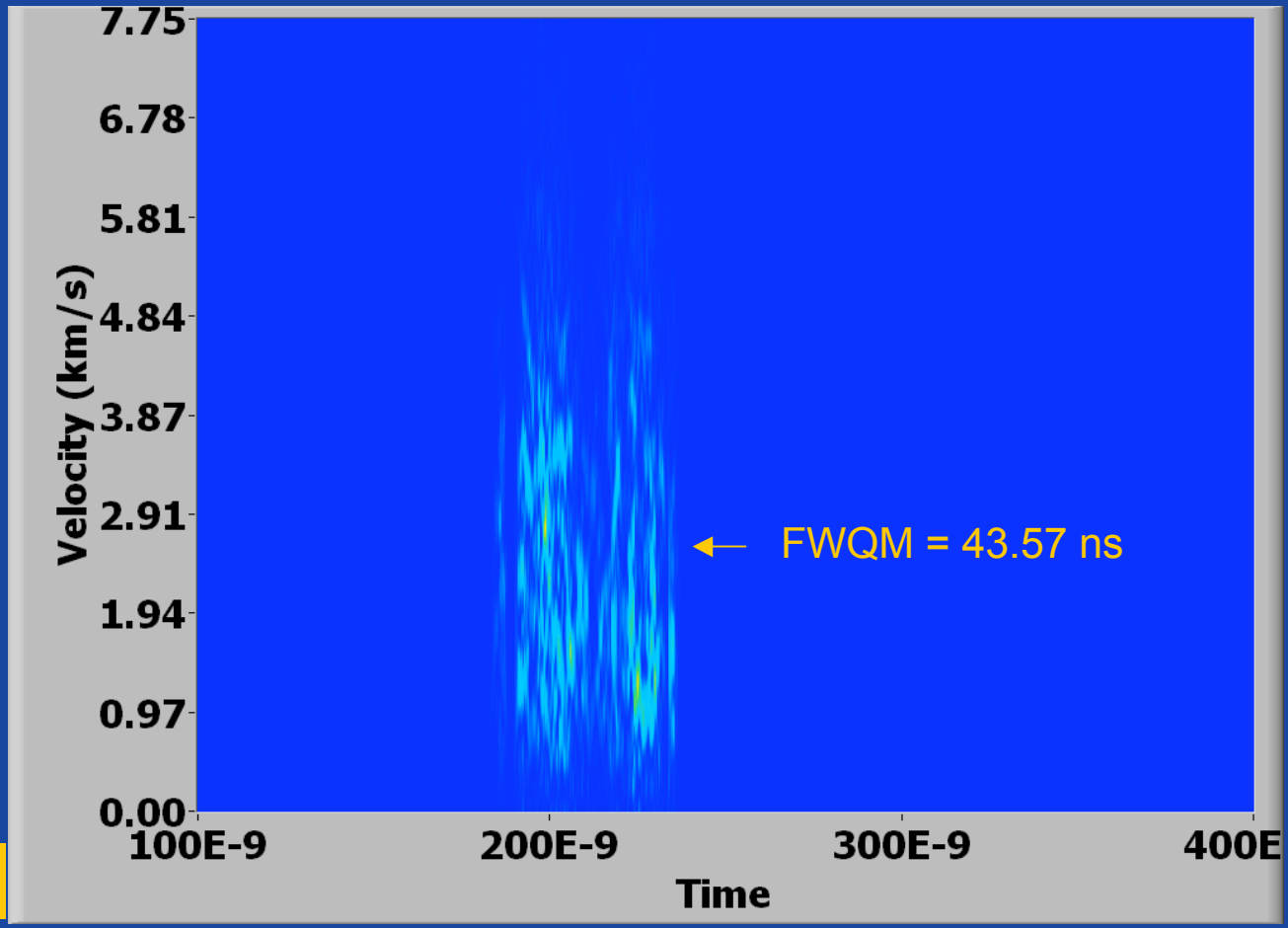

Fluence = 4.85 J/cm^2

PDV on Au Target

Longer temporal data and evolving velocity data.

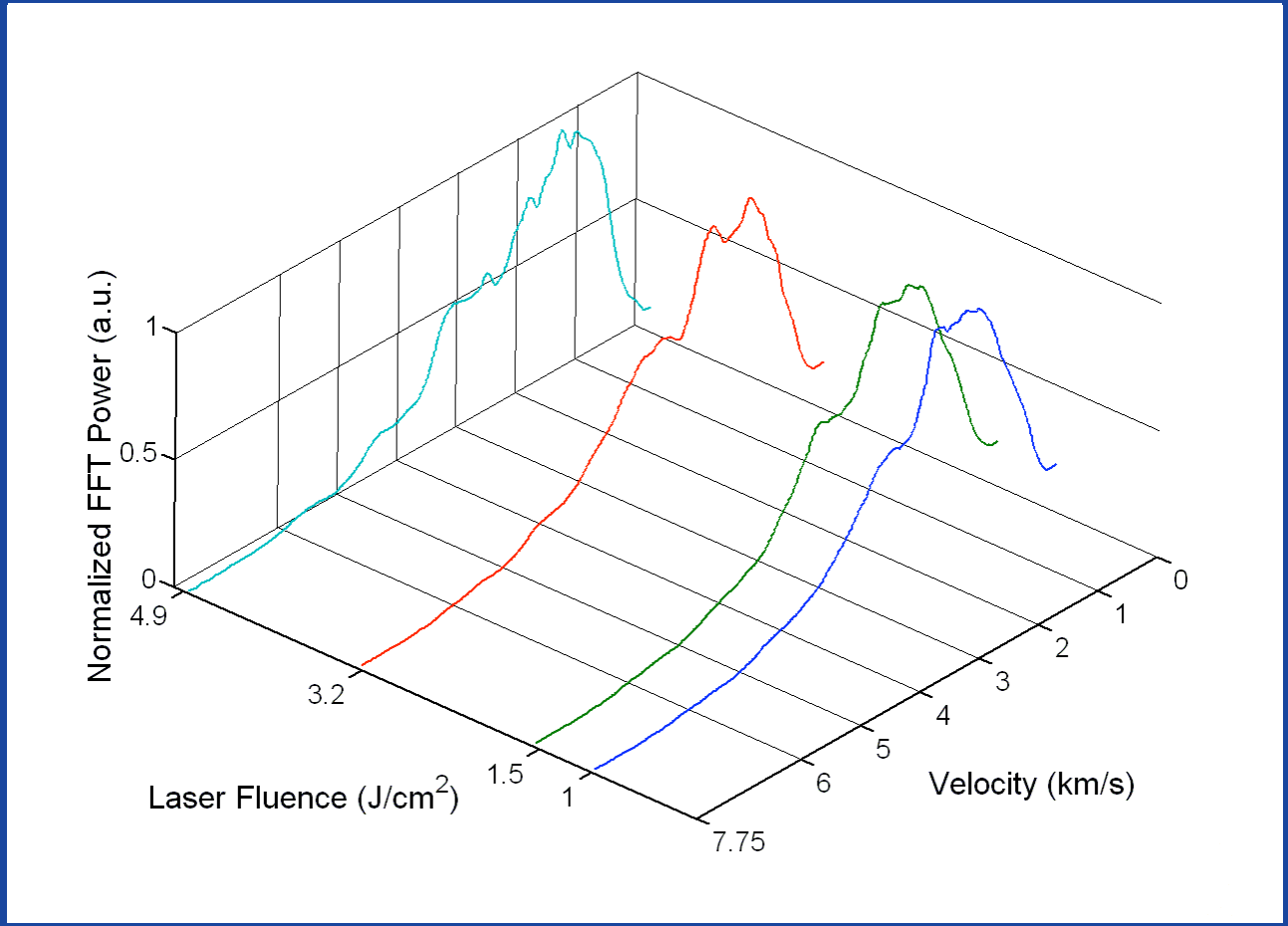

Thoughts on Analysis Methods

- Without long time-continuous frequency components, it is difficult to recover multiple velocity field distributions using STFT alone.
- Despite using the STFT for calculation of most of our spectrograms, we have begun exploring additional transforms for analysis: Gabor, Wigner-Ville and Wavelets.
- Wavelet seem like an attractive method as they provide multiple frequency & time scale resolution capability
- Additionally pre-spectrogram low frequency denoising can also be accomplished with wavelet filtering.

Typical High-Freq Example: 100 nm Au on 20 μm parylene

- **To date, much of our data has been analyzed using the normal ST-FFT transform with narrow time windows (16 - 32 pts ~ 2 - 4 ns) processing focusing in on high frequency response.**

$$STFT(t,\omega) = \int s(\tau)\gamma(t-\tau)e^{-j\omega\tau}d\tau$$

$\gamma(t-\tau)$: unit square window function

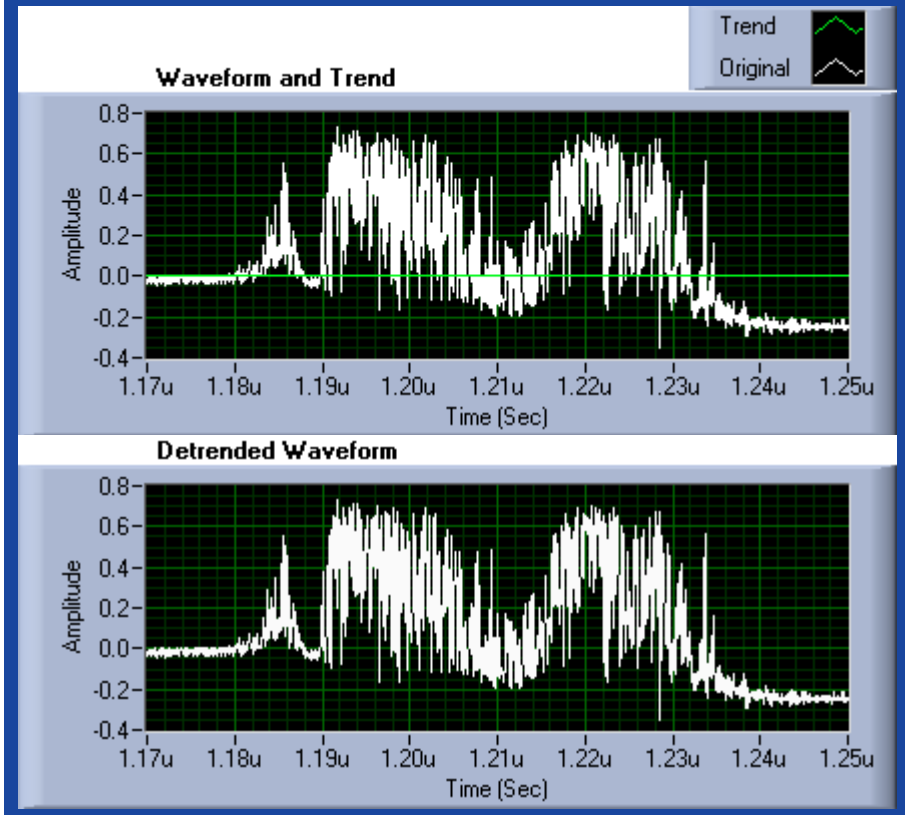

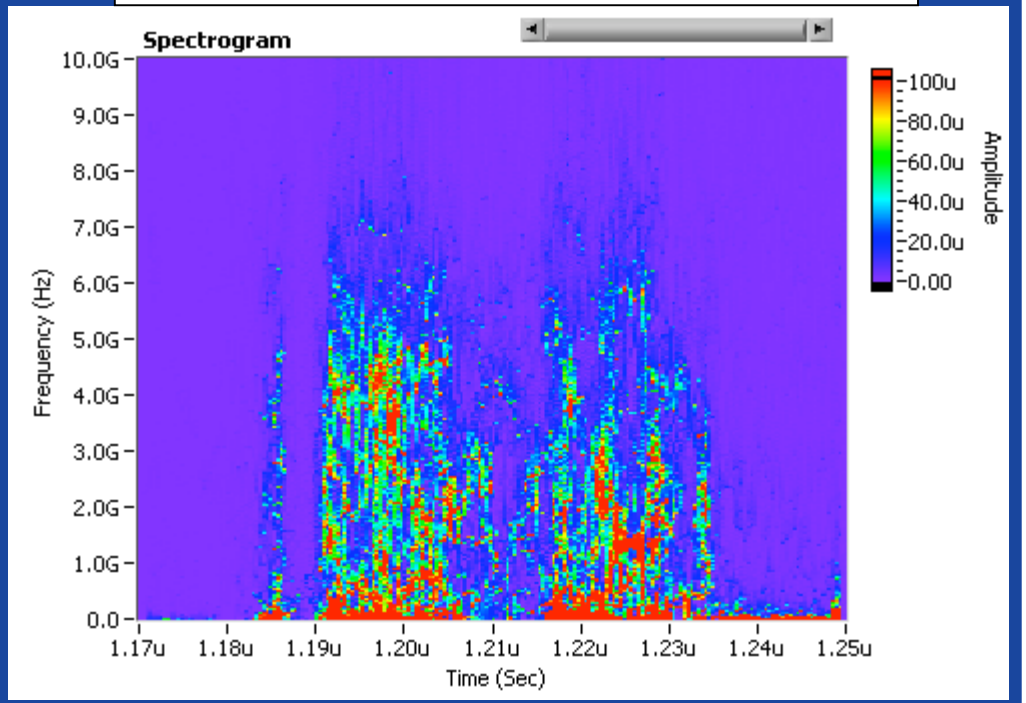

Gabor and Wigner-Ville Transform of short-time multiple-frequency signals

- **Our experience with other transforms such as Gabor and Wigner-Ville transforms are showing that detailed information on multiple-frequency short-time scales do not show much improvement over the ST-FFT.**

$$GT(t,\omega) = \int s(\tau)\gamma(t-\tau)e^{-j\omega\tau}d\tau$$

$$\gamma(t-\tau) = \exp\left[-\frac{(t-\tau)^2}{2\sigma^2}\right]$$

$$WVT(t,\omega) = \int s(t+\tau/2)\cdot s^*(t-\tau/2)e^{-j\omega\tau}d\tau$$

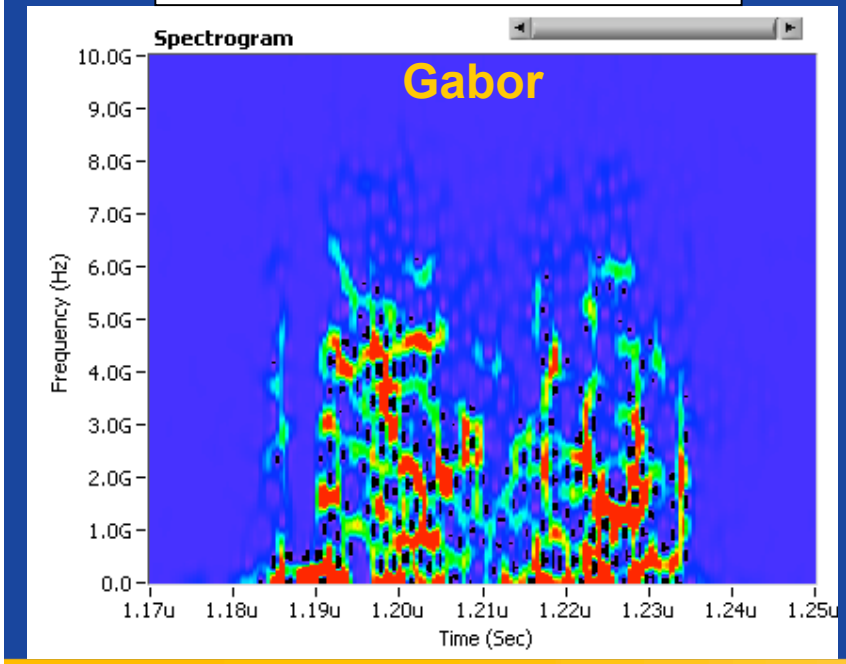

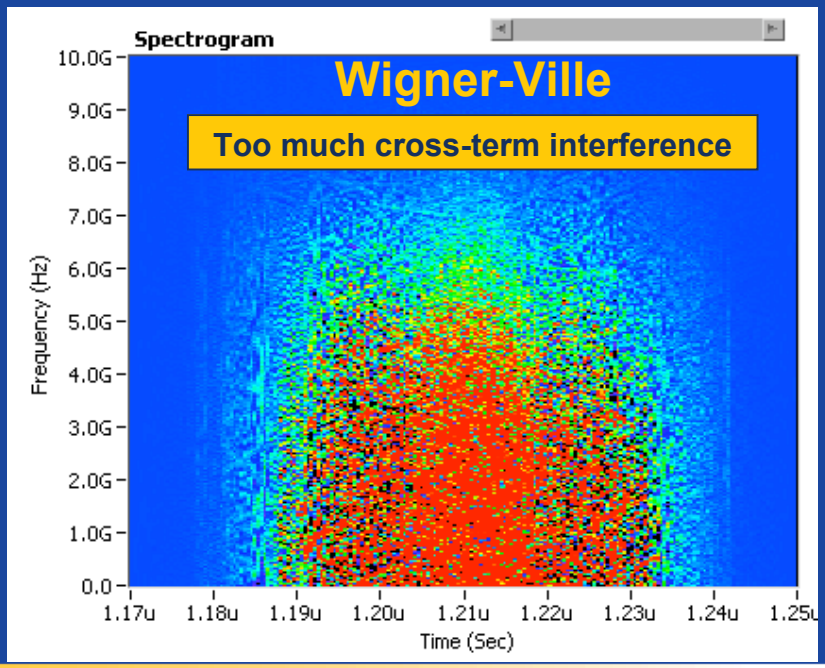

Wavelet transform may have an advantage due to their multiple scale (scalogram vs. spectrogram) representation

- **Wavelet transform provides method to extract multiple scale signals in producing its corresponding scalogram.**
- **We use Morlet function as basis wavelet, ψ :**

$$\psi(t) = \frac{1}{\sqrt{2\pi a}} e^{-\frac{t^2}{2a^2}} e^{-i\frac{2\pi\omega_0 t}{a}}$$

where first scale, $a = 2\omega_0$

$$WT(a,b) = \frac{1}{\sqrt{a}} \int s(\tau)\psi^*\left(\frac{\tau - a}{b}\right) d\tau$$

ψ : wavelet function

a : scale factor

b : sampling step, $\quad \omega \sim 1/b$

Spectrogram

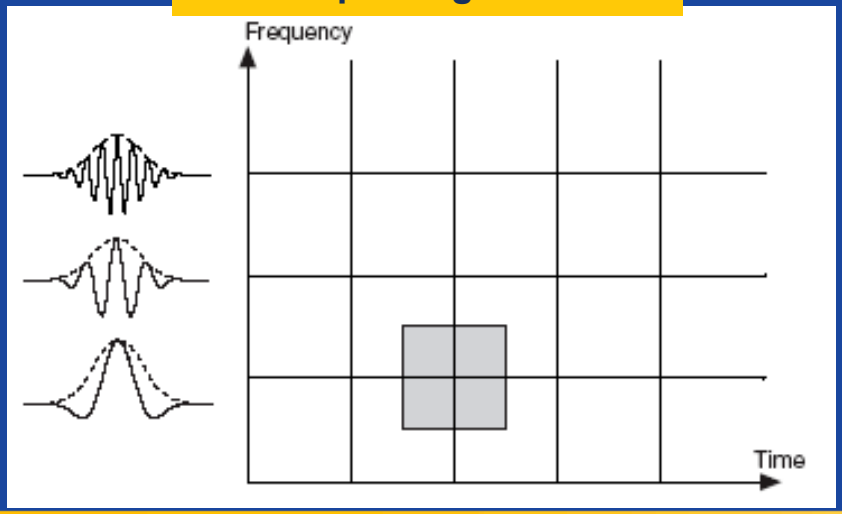

Wavelet Scalogram

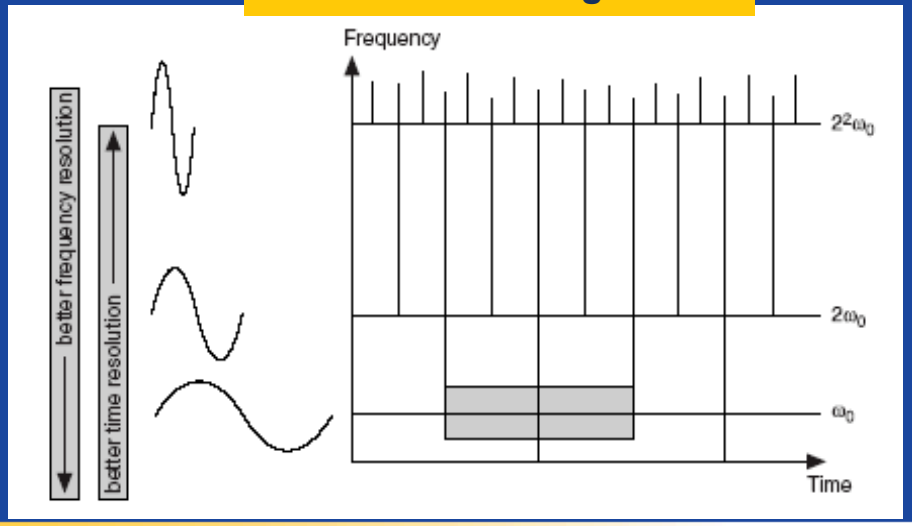

Multi- resolution wavelet example: 10 μm Al foil @ 4.84 J/cm²

Raw Data has strong heterodyne signal at ~ 45 MHz

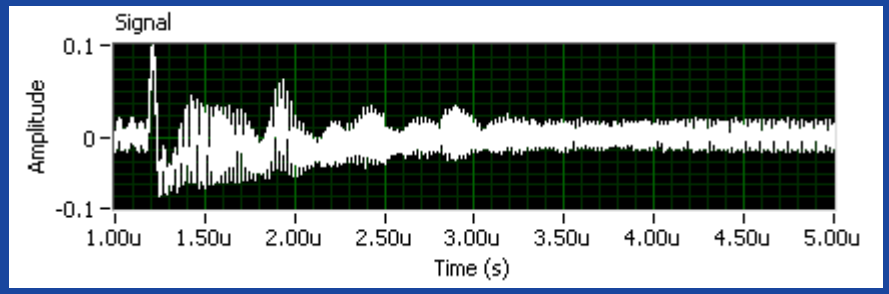

Wavelet transform is computed at 4096 scales

Wavelet Transform Scale vs. Time

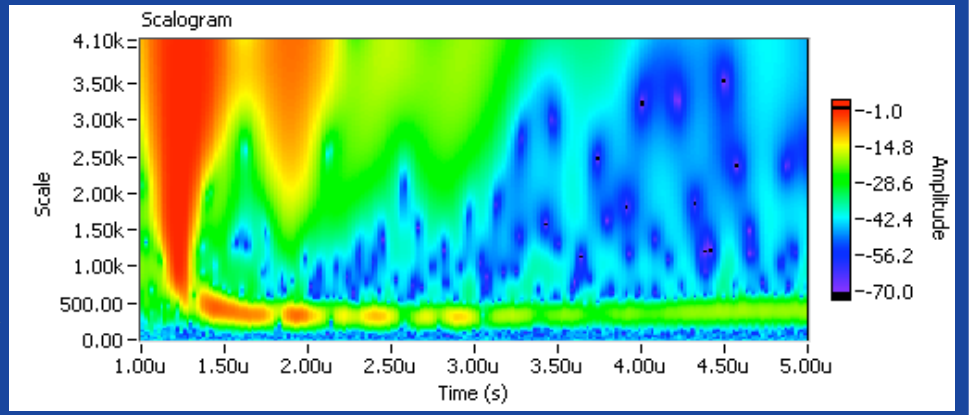

Low frequency portion is extracted velocity ~ 35 m/sec

Wavelet Transform Frequency vs. Time

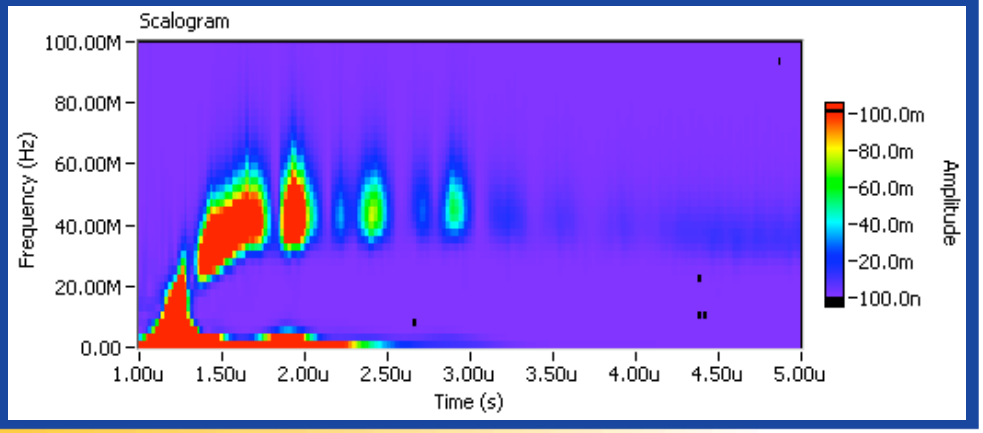

High-Freq Wavelet Example: 100 nm Au on 20 μm parylene

- **Our wavelet transform analysis shows that comparable to better time resolution is achieved with wavelet transform.**

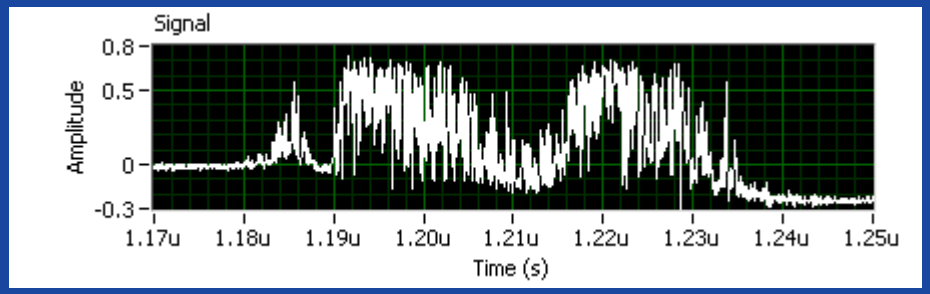

STFT Spectrogram

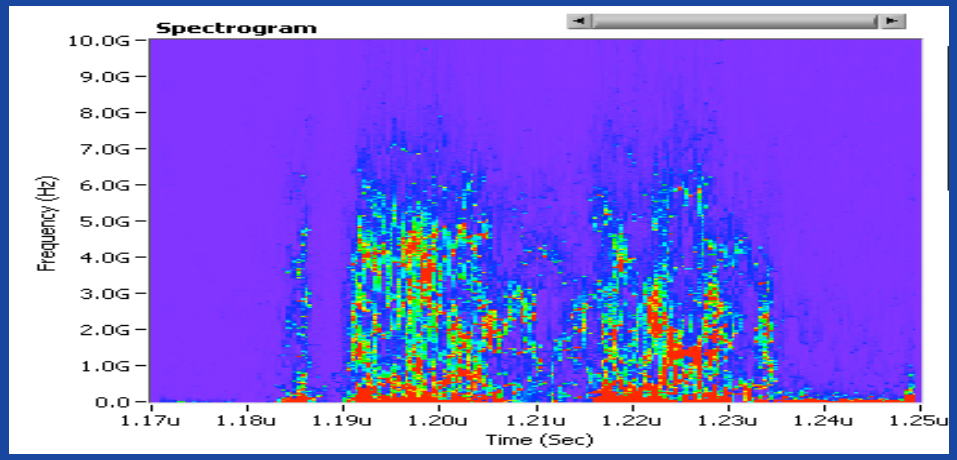

Wavelet Scalogram

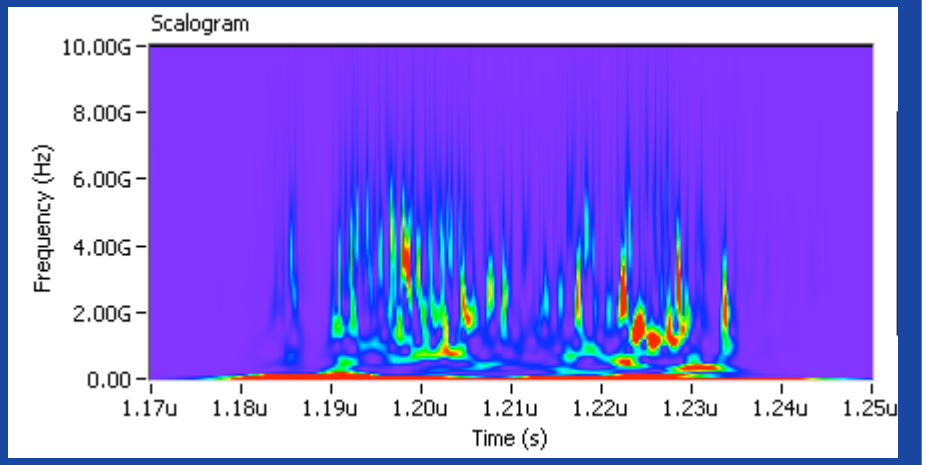

Low Frequency Wavelet Denoising Example

- Normal STFT processing (w/o wavelet detrending) shows that a ~45MHz frequency carries with it significant near DC power.
- Difficult to remove fully using standard FIR filtering.

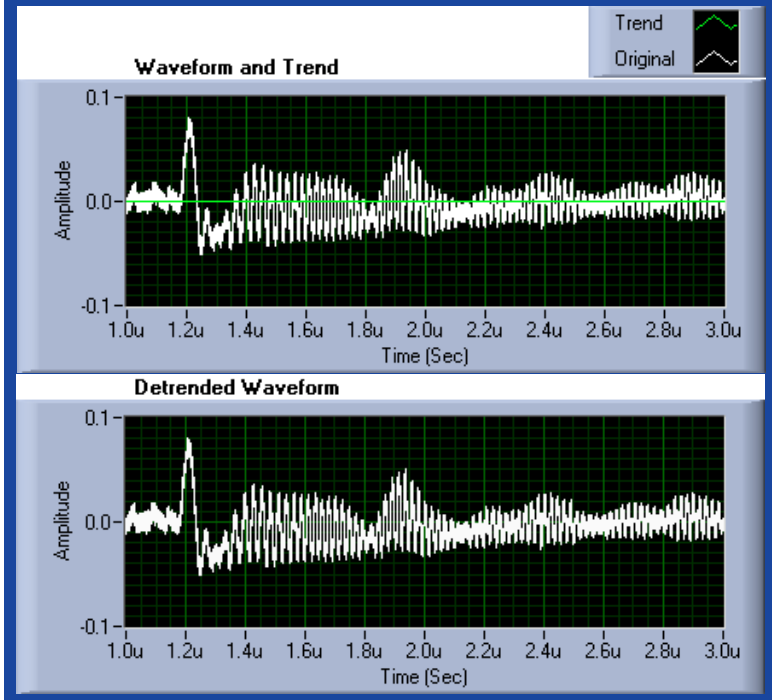

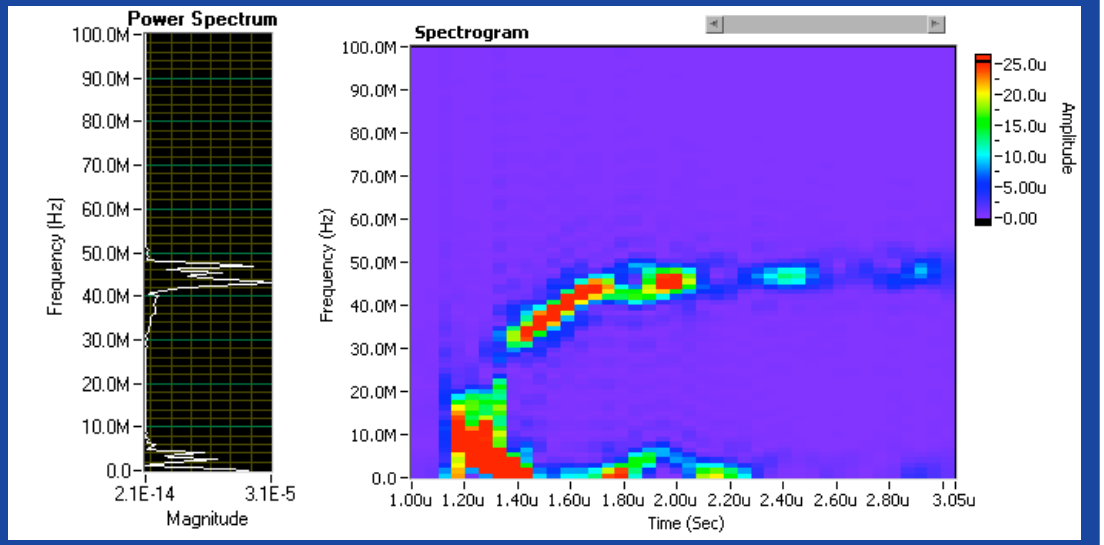

Low Frequency Denoising Example

- After wavelet (Bior2_8) pre-processing, STFT spectrogram becomes "cleaner" maintaining main 45 MHz features.
- Result: Very low velocity (~ 35 m/sec) feature are faithfully recovered.
- We think these are drum like mechanical vibrations from 10 um Al substrate after ablation.

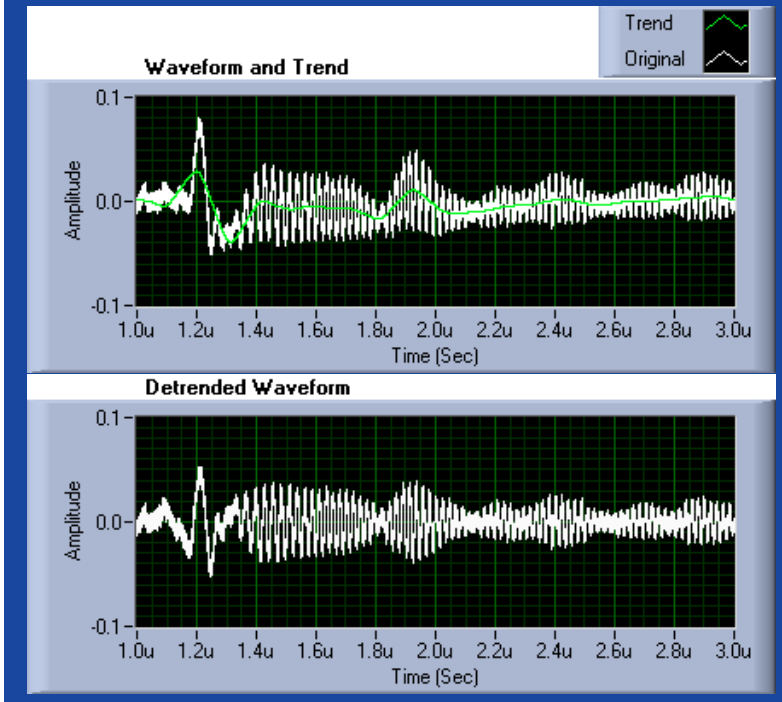

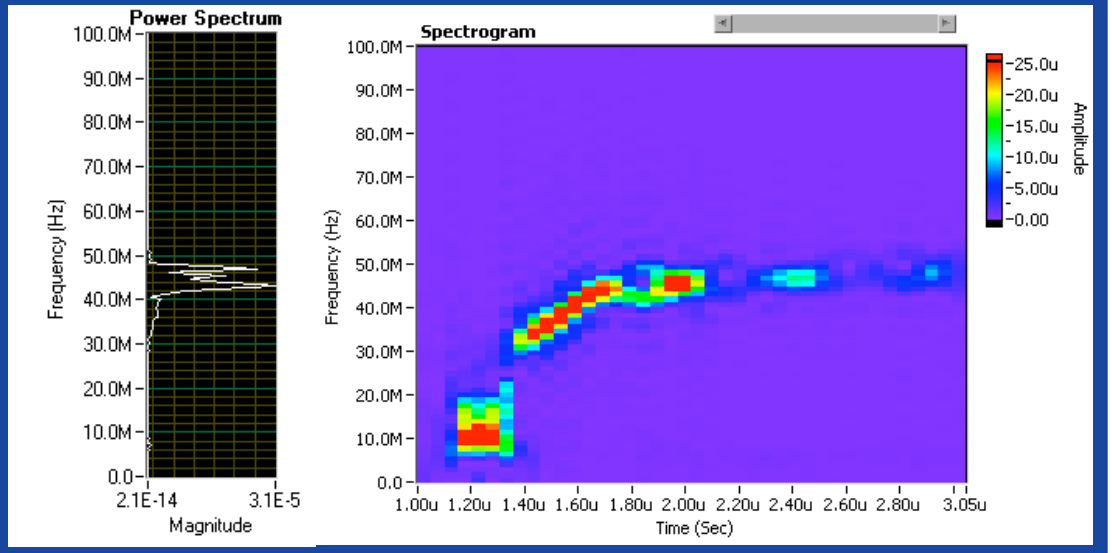

Summary/Final Thoughts

- Heterodyne velocimetry clearly has its advantages over VISAR as its ability to track multiple velocity fields in laser ablation is demonstrated.
- Still yet higher bandwidth systems are needed to fully track ablated and ejected particles at highest velocities.
- Switch over to very small probe spot size dimensions show only a modest improvement in bandwidth (may be due to electronic detection bandwidth limitations).
- Combination of multiple frequency and high time resolution clearly represents challenge to standard STFT analysis. Wavelets may help in the case, and in the case of data filtering.

Laser Radiation Hydrodynamic Code

We utilized HYADES hydrodynamic and energy transport code that features:

- 1-D Lagrangian hydro and 3-temperature (T_e, T_i, T_r)
- LTE fluid approximation (Maxwell-Boltzmann) with $T_i \neq T_e$
- Sesame EOS and QEOS
- Material strength, spall and melt models
- Ionization
- Laser absorption & deposition

Physics of Simulation

The fluence threshold (F_{th}) for ablation of a bulk metal is principally determined by the thermal diffusivity (a), laser pulse width (τ), and heat of vaporization (L_v):

$$F_{th} = \rho L_v \sqrt{a\tau} \quad \text{(bulk)}$$

For titanium: ρ = 4.54 g/cm^3, L_v=421 kJ/mol, a = 0.0928 cm^2/s, and τ = 15 ns laser pulse.

$$F_{th} = 1.49 \text{ J/cm}^2 \quad \text{(bulk)}$$

Yet, thermal diffusion length,

$$L_{th} = \sqrt{a\tau} = 373 \text{ nm}$$

is longer than film thickness, d ~250 nm. Therefore, for a film, we replace the L_{th} with d:

$$F_{th} = \rho L_v d \quad \text{(film)}$$

$$F_{th} = 0.998 \text{ J/cm}^2 \quad \text{(film)}$$

Calculated Density, Pressure and Temperature

Time snapshots of the calculated distributions at a laser fluence of 3.26 J/cm^2 for a) the density across entire glass-titanium target, b) the pressure distribution across titanium layer (zone index positions 125 to 200) and c) temperature across the interface. The 15-ns laser pulse is time centered to have a maximum intensity at t = 30 ns.

c)

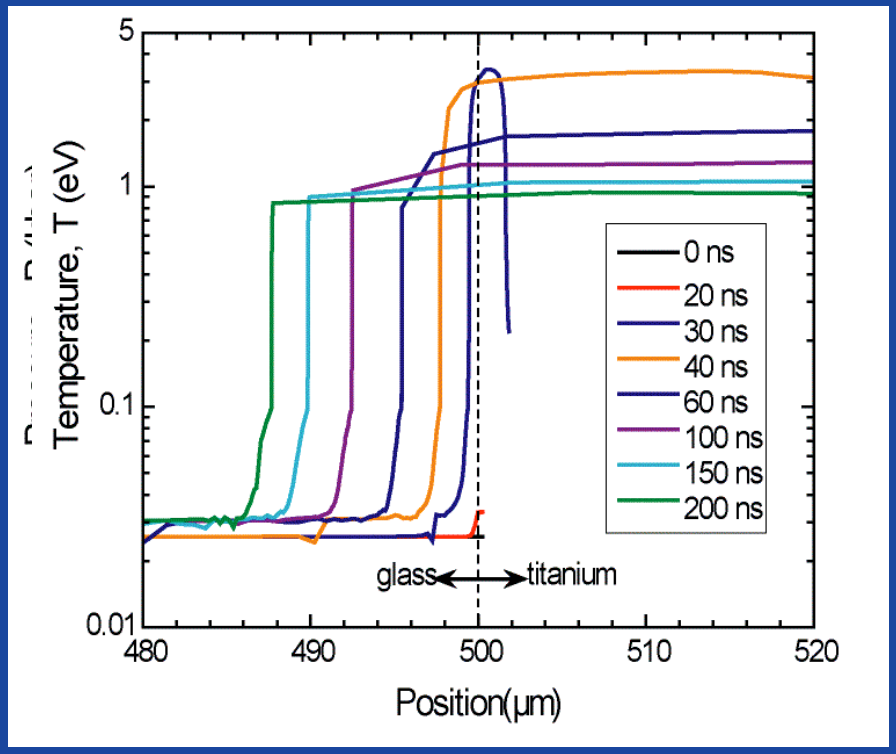

Surface Expansion versus Fluence

Calculated free surface hydrodynamic displacement as a function of time near the glass-titanium interface for various laser pulse fluences: a) 0.3 J/cm^2; b) 1.6 J/cm^2; c) 3.3 J/cm^2; (d) 8.2 J/cm^2. The 15-ns laser pulse is time centered to have a maximum intensity at τ = 30 ns.

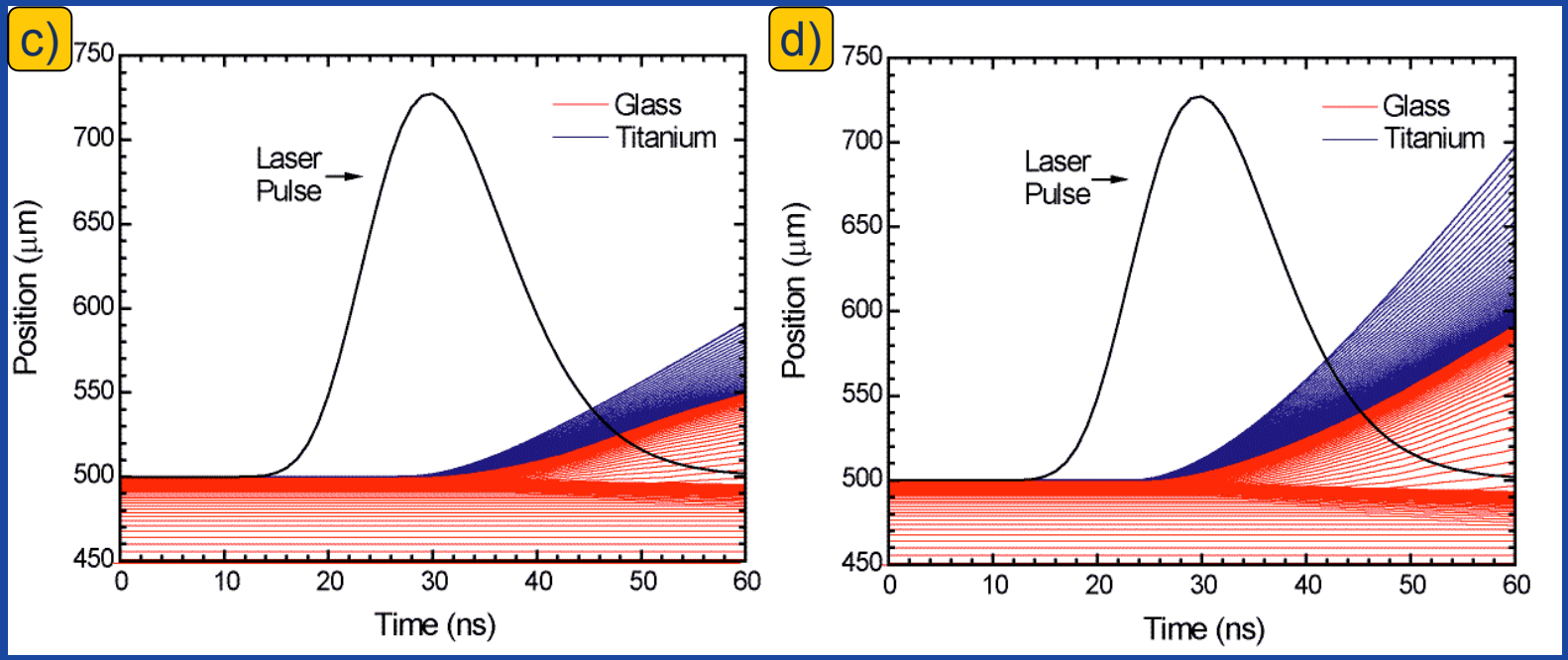

Calculated Surface Velocity

Calculated expansion velocity of the titanium layer for several laser fluences. The calculation assumes a 250 nm (solid curves) or a 350 nm (dashed curves) layer of titanium.

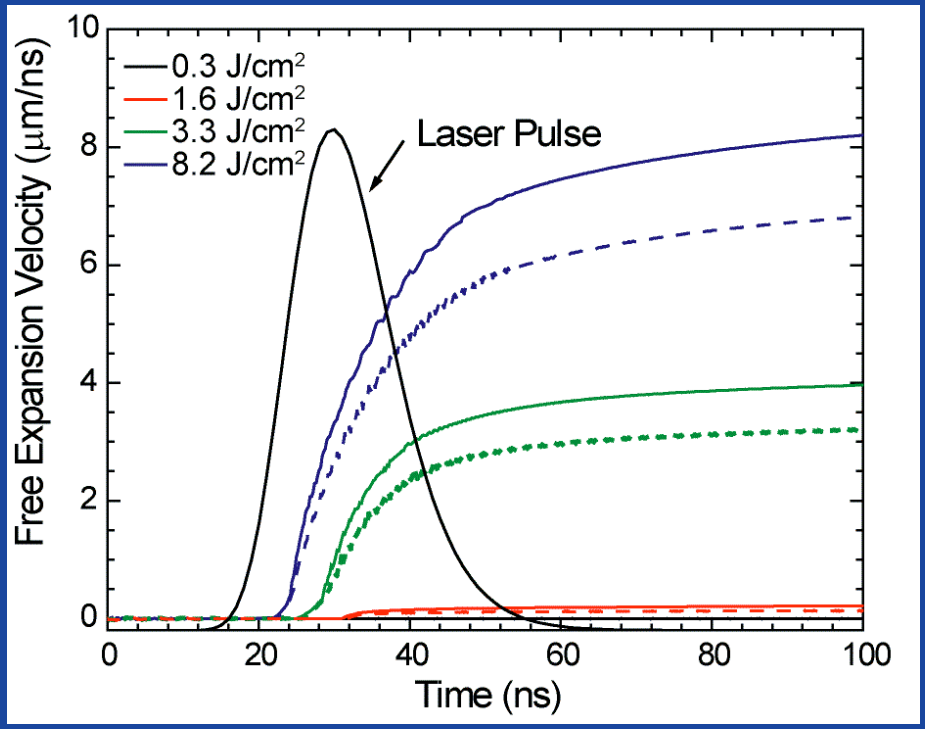

Summary: HYADES Calculations

- HYADES calculations predict that Ti layer undergoes melt and additional heating via thermal conduction during the laser pulse duration
- A warm plasma and molten metal approaching several eV (~3.5 eV) at pressures of ~ 30 kbar is created and subsequent expansion of molten material and plasma is calculated.
- Initial velocimetry experiments confirm that terminal velocity is achieved at near the end of the laser pulse with free surface velocities approaching 6 μm/ns are readily achieved into free space.
- PDV measurements consistently measure a spread of velocities as ejected material is launched from several spatial positions across the laser spot size.
- Parametric (i.e., laser fluence vs. velocity) studies show that peak velocities in the PDV spectrogram are consistent with HYADES calculations.
- 2-D time-resolved DOTS topographic mapping/imaging experiments are underway.

Acknowledgements

This work is funded by the Direct Optical Initiation Project under the Joint Munitions DoD/DOE Program at Los Alamos National Laboratory. Additional funding is also provided by Los Alamos National Security LLC Laboratory Directed Research and Development Program at Los Alamos National Laboratory under auspices of the Department of Energy contract number DE-AC52-06NA25396.

References

- B. N. Chichkov, C. Momma, S. Nolte, F. V. Alvensleben, and A. Tunnermann, “Femtosecond, picosecond, and nanosecond laser ablation of solids," *Appl. Phys. A* **63**, p. 109, 1996.
- B. C. Platt and R. Shack, “History and principles of Shack-Hartmann wavefront sensing," *Journal of Ref. Surgery* **17**, p. S573, 2001.
- O. T. Strand, L. V. Berzins, D. R. Goosman, W. W. Kuhlow, P. R. Sargis, and T. Whitworth, “Velocimetry using heterodyne techniques," in *26th International Conference on High-Speed Photography and Photonics*, (Alexandria, VA), 2004. Conference Report UCRL-CONF-206034.